Self-Assembled Monolayers of Novel Surface-Bound Dendrons: Peripheral Structure Determines Surface Organization

Bin Dong,[a] Fengwei Huo,[a] Lu Zhang,[a] Xunyu Yang,[a] Zhiqiang Wang,[a] Xi Zhang,*[a] Shaoyun Gong,[b] and Jinghong Li[b]

Abstract: The synthetic and functional versatility of dendrimers and their well-defined shapes make them attractive molecules for surface modification. We synthesized six structurally very similar surface-bound dendrons and used them as building blocks for the preparation of self-assembled monolayers (SAMs) on a gold surface. We studied the effects of the surface-bound dendron's main structure, peripheral substituents, and the coadsorption process on its self-assembling behavior. Using scanning tunneling microscopy (STM), we observed nanostripes for SAMs of the surface-bound dendron consisting of symmetrical benzene rings. When we changed the symmetrical dendron's structure slightly, by increasing or decreasing the numbers of benzene rings at one wedge, we found no ordered structures were formed by the asymmetrical dendrons. We also introduced two kinds of substituents, heptane chains and oligo(ethylene oxide) chains, to the symmetrical dendron's periphery. Heptane chains appear to enhance the interaction between symmetrical backbones, leading to the formation of stripes, while oligo(ethylene oxide) chains appear to weaken the interaction between symmetrical backbones, resulting in a homogeneous structure. Dendrons with both heptane and oligo(ethylene oxide) chains exhibit nanophase separation in a confined state, leading to the formation of a honeycomb structure. Electrochemical studies provide additional evidence for understanding the resulting surface organizations: surface-bound dendrons with symmetrical structures form denser monolayers than their asymmetrical analogues; SAMs comprising peripherally substituted dendrons exhibit blocking effects proportionate to their hydrophilic fraction.

Keywords: dendrimers · electrochemistry · scanning tunneling microscopy · self-assembled monolayers · surface chemistry

Introduction

Dendrimers, as macromolecules with globular shape and unusual physical properties, have attracted more and more attention since their discovery.[1] Research has ranged from the synthesis of dendrimers to different methods of functionalizing their focal point, branching units, and periphery. The possibilities of using dendrimers as building blocks in catalysis,[2, 3] pharmacology,[4] and materials science have been explored. As surface chemistry becomes increasingly important, dendrimers like surface-bound dendrons become more attractive. For example, Fréchet et al. have demonstrated that the mixed monolayer of donor and acceptor chromophore surface-bound dendrons may result in the emission amplification through energy transfer between donor and acceptor.[5] Fréchet's group also proved that a polyether dendron can be used for high-resolution scanning probe lithography (SPL) on a silica surface.[6, 7]

Thiol/gold systems[8–10] are of great interest with respect to obtaining a better understanding of the self-assembling phenomena at their interfaces as well as for their applications in functional materials.[11–13] Using dendrons with a focal thiol substituent, Gorman[14] and co-workers assembled monolayers of first-, second-, and third-generation dendrons on gold surfaces. In addition, Zhang and Chi et al. have synthesized a series of surface-bound dendrons and studied the surface morphology of these dendrons on the Au (111) surface in detail by using STM.[15–17]

Herein, we report the STM and electrochemical study of SAMs attached to a novel surface-bound dendron system, which maintains the active sites of the alkanethiols, but with

[a] Prof. Dr. X. Zhang, B. Dong, F. Huo, L. Zhang, X. Yang, Dr. Z. Wang
Key Lab of Supramolecular Structure & Materials
College of Chemistry, Jilin University
Changchun 130023 (P. R. China)
Fax: (+86) 431-8980729
E-mail: xi@jlu.edu.cn

[b] S. Gong, Prof. Dr. J. Li
State Key Lab of Electroanalytical Chemistry
Changchun Institute of Applied Chemistry
Chinese Academy of Sciences
Changchun 130022 (P. R. China)

 DOI: 10.1002/chem.200204483

the -SH group connected to variable groups by a dendritic linkage. By designing the dendritic part, we can fabricate a series of surface-bound dendrons with structures slightly different from each other. Such tiny differences should enable us to monitor the way molecular structure modifies surface organization. Because technological applications may rely on materials containing mixed monolayers comprising two or more components, we also consider the coadsorption process.

Results

Design and synthesis of two groups of surface-bound dendrons: To compare the influence of symmetrical and asymmetrical structure of dendrons on surface organization, we took the convergent synthesis route to synthesize well-defined dendritic structures in nonparallel ways (Scheme 1). By controlling the reaction of the wedge with a large excess of monomer, we generated a half-reacted branching unit. Another wedge was then attached to the other dendron branch, creating another branching unit with different functionalities on each of its branches.[18–20] By using this method, we synthesized a series of asymmetrical dendrons (D1,3 and D3,7 in Scheme 1) with different benzene rings on each of its sides. We also synthesized symmetric dendrons (D3,3 in Scheme 1) for comparison.

Based on the same backbone as the symmetrical dendron D3,3, we introduced two types of building blocks with different hydrophobicity at the dendron's periphery (Scheme 2). Surface-bound dendrons with both hydrophobic heptane chains (R) and hydrophilic oligo(ethylene oxide) chains (EO) at their periphery were synthesized in a nonparallel way, and labeled as G2REO (Scheme 2). For comparison, we also synthesized surface-bound dendrons with either hydrophobic or hydrophilic groups at their periphery, labeled as G2R and G2EO (Scheme 2), respectively. We expect that SAMs of these surface-bound dendrons with locally controlled hydrophobicity will enable us to detect the effect of peripheral substituents on the dendron's aggregation behavior.

SAMs of surface-bound dendrons with symmetrical or asymmetrical peripheral structures: We used STM to study the series of SAMs of surface-bound dendrons D1,3, D3,3 and D3,7. The dendron with symmetrical structures (D3,3) can form a highly ordered stripe pattern, with stripes approximately 3.1 ± 0.3 nm wide (Figure 1b). The long-range order is ascribable to the chemisorption between the thiol group and the gold surface, and to the $\pi-\pi$ stacking between benzene rings.[16] For dendrons with asymmetrical structures (D1,3 and D3,7; Scheme 1), we only observed random pore structures; the pore sizes ranged from 6 to 13 nm and 4 to 9 nm, respectively (Figure 1a and 1c). We assume that the lack of symmetrical structure may result in defects in between these asymmetrical surface-bound dendrons when two or more molecules pack together with end-on configuration. This mismatch may also disturb the factors (such as $\pi-\pi$ stacking) responsible for the long-range order. It is difficult to distinguish the two asymmetrical surface-bound dendrons through the STM images, although there are some differences between their molecular structures. We conclude that the symmetrical structure of dendron D3,3 plays an important role in the formation of the stripe pattern for the SAMs of this first series of dendrons.

Electrochemical measurements were also used performed on the SAMs of these surface-bound dendrons. In Figure 2, the peak current I_p and the fraction of pinhole area $(1-\Theta)$ of D1,3 (B) and D3,7 (C) are larger than that of D3,3(D), which indicates that the electron exchange process

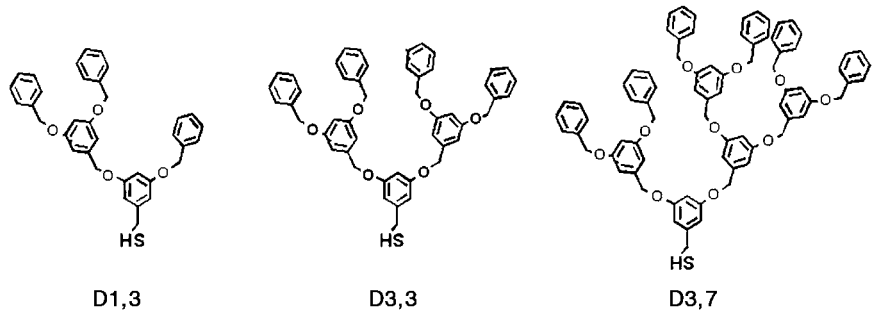

Scheme 1. Chemical structures of asymmetric and symmetric surface-bound dendrons.

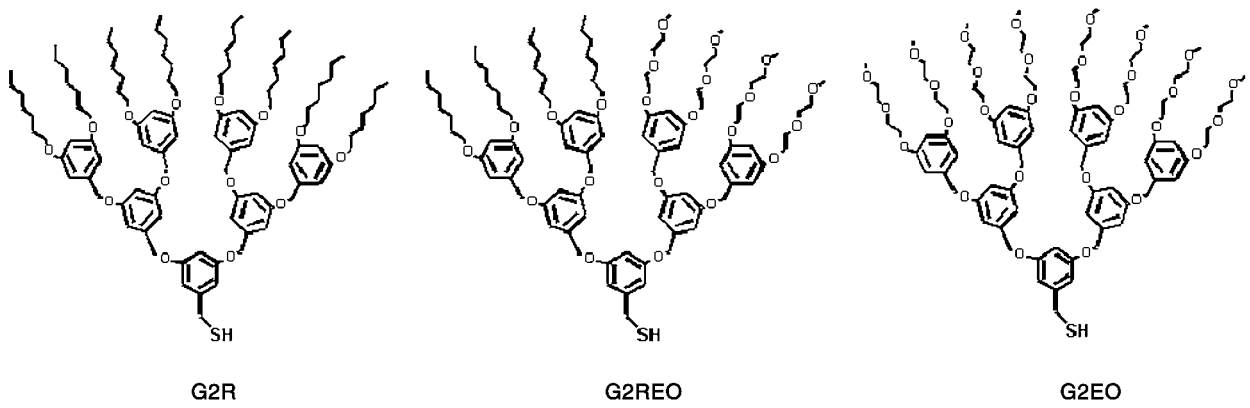

Scheme 2. Chemical structures of surface-bound dendrons bearing different substituents with different hydrophobicity at the periphery.

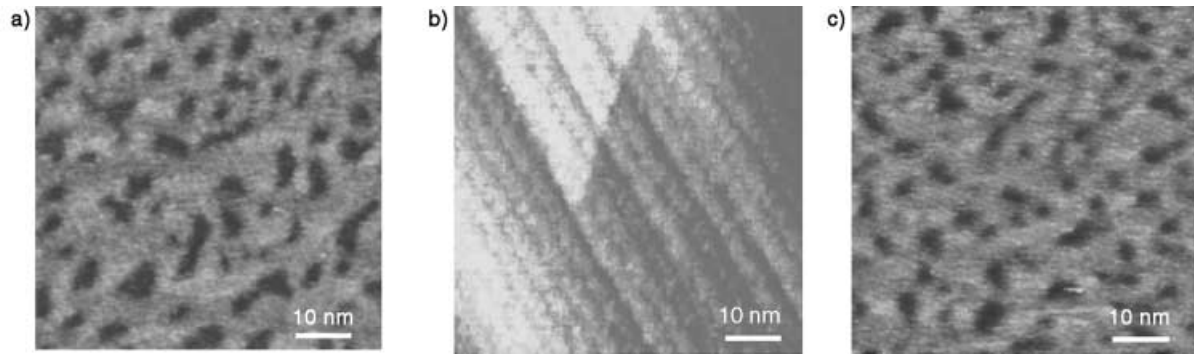

Figure 1. STM images of SAMs of asymmetric surface-bound dendron D1,3 (a), symmetric surface-bound dendron D3,3 (b), and asymmetric surface-bound dendron D3,7 (c) on a gold surface.

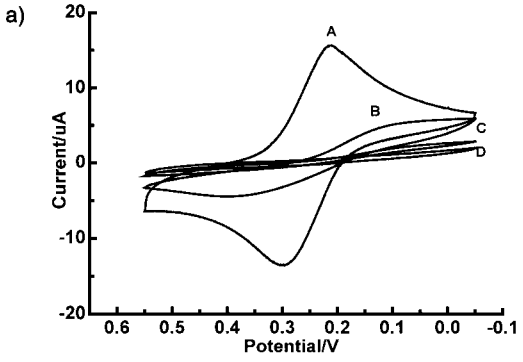

b)

	Au(A)	D1,3(B)	D3,7(C)	D3,3(D)
E_{pc}/V	0.211(0.008)	0.111(0.007)	0.061(0.008)	0.053(0.012)
E_{pa}/V	0.299(0.011)	0.402(0.015)	0.486(0.013)	0.510(0.021)
I_{pc}/(μA)	13.0(0.5)	1.87(0.10)	0.30(0.05)	0.29(0.05)
I_{pa}/(μA)	-14.0(0.8)	-2.18(0.08)	-0.28(0.07)	-0.24(0.08)
ΔE_p/V	0.088	0.291	0.425	0.457
(1- Θ)		0.209	0.030	0.024
C_{dl}/(10^{-8}F)		58.18(3.21)	10.14(1.32)	8.977(0.586)
C_m/(10^{-8}F)		2.741	2.165	2.608
d/nm		1.5	1.9	1.6

Figure 2. a) Cyclic voltammograms of bare Au (A), D1,3/Au (B), D3,7/Au (C), D3,3/Au (D) in a solution of 2 mM $K_3[Fe(CN)_6]$ + 0.1 M KCl at a scan rate of 0.10 V s^{-1}; b) Voltammetric results summarized for SAMs.

becomes easier for asymmetrical surface-bound dendrons than for symmetrical ones. A possible reason is that the mismatch existed in the structure of asymmetrical surface-bound dendron, and led to the formation of defects, resulting in the decrease of blocking effect. Moreover, it seems that the defects are fewer when the generation of substituted wedge at each side increased (Note that the ΔE_p of D3,7 is larger than that of D1,3). On the contrary, the symmetrical chemical structure of D3,3 enables the denser molecular packing, showing the strongest blocking effect (Figure 2). Furthermore, based on the capacitance, the monolayer thickness can be calculated as shown in Figure 2b.

We used the equivalent circuit model (Figure 3 inset) to simulate the complex impedance plots of D1,3/Au obtained from electrochemical impedance spectroscopy (EIS) measurements. The curve (solid line in Figure 3) fits well with the experimental impedance data (solid square in Figure 3), which indicates that the equivalent circuit used is accurate.

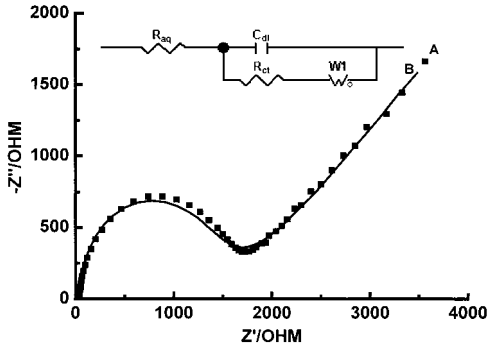

Figure 3. Simulated result of D1,3/Au by applying equivalent circuit model. The solid square (A) is the complex impedance plot of D1,3/Au, and the solid line (B) is the simulated result of D1,3/Au. Inset: Equivalent circuit model for complex impedance plots. R_{aq} is the solution resistance. C_{dl} represents the dendron monolayer/solution interface capacitance. R_{ct} is the charge transfer resistance due to electron transfer at the monolayer/solution interface. W1 is the Warburg diffusion impedance.

As the surface-bound dendrons pack more densely, their diameters become larger (Figure 4a) and the charge transferring velocity constant k^o smaller (Figure 4 b) from D1,3/Au to D3,7/Au to D3,3/Au, showing the increase in the blocking effect, changes which are consistent with cyclic voltammetric data.

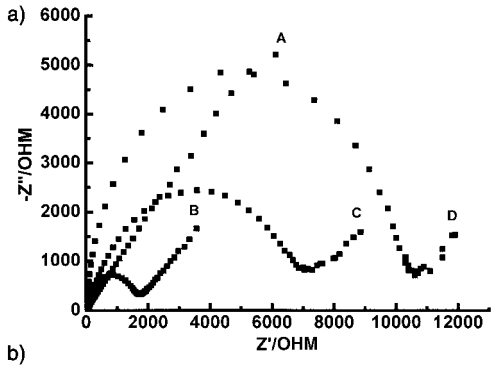

b)

	D1,3(B)	D3,7(C)	D3,3(D)
R_{aq} /Ω	37.3(9.1)	46.1(8.5)	36.7(5.8)
R_{ct} /Ω	1269(50)	6250(65)	9824(82)
k^o/(10^{-6} m s^{-1})	13.4	2.7	1.7

Figure 4. a) Complex impedance plots of bare Au (A), D1,3/Au (B), D3,7/Au (C), and D3,3/Au (D) electrodes in 5 mM $K_4[Fe(CN)_6]$ + 5 mM $K_3[Fe(CN)_6]$ + 0.5 M KCl aqueous solution. b) AC impedance results for the electrodes.

SAMs of surface-bound dendron with different substituents at periphery: For the series of the surface-bound dendrons G2R, G2EO, and G2REO, the main skeletons are the same as D3,3 but their peripheries differ. The different periphery is, therefore, the main factor influencing the intermolecular interaction of the D3,3 skeleton. We used STM to observe the surface morphology of SAMs of G2R, G2EO, and G2REO on Au(111). For the dendrons with purely hydrophobic peripheries (G2R) as building blocks, the SAMs on the gold surface display striped structures as shown in Figure 5a. The width of the stripes is approximately 4.0 ± 0.5 nm. In comparison with D3,3, the hydrophobic interactions among the peripheral heptane chains in G2R as well as the chemisorption and the $\pi-\pi$ stacking contribute to the expansion of the stripe width and to some extent to the stripes' long-range order. For SAMs of G2EO bearing a hydrophilic periphery, only a homogeneous surface structure (except for a few defects) could be observed on Au(111) (Figure 5b). The possible reason is that the interaction between the D3,3 skeleton is weakened by the conformation of the EO chain.

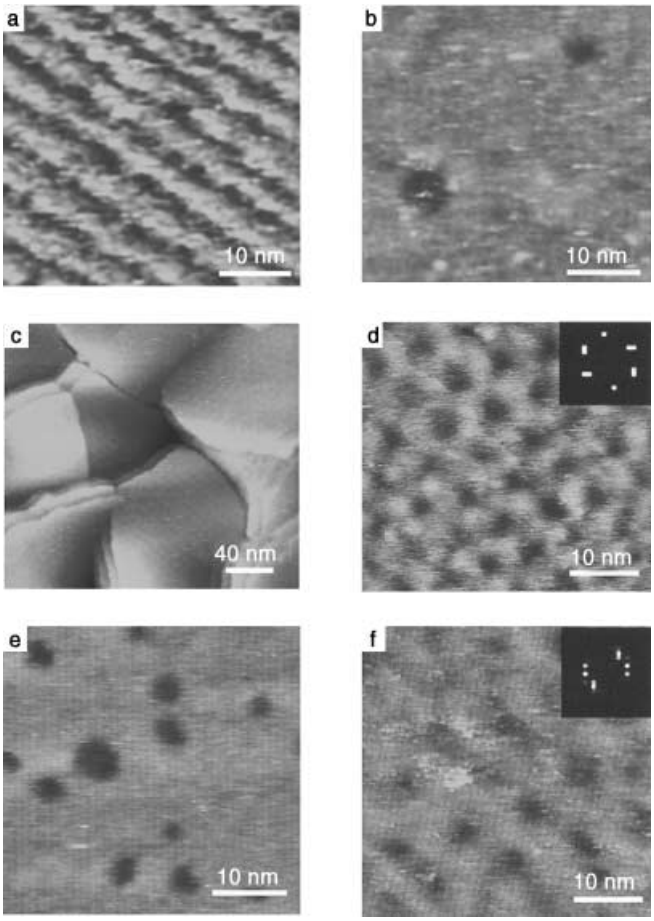

Figure 5. STM images of SAMs of surface-bound dendron on gold surface a) G2R, b) G2EO, c) G2REO magnified, d) G2REO at low resolution (inset: spectrum 2D image), e) 1:1 mixture of G2R and G2EO, f) 20:1 mixture of G2REO and G2R (inset: spectrum 2D image).

SAMs of surface-bound dendrons bearing both hydrophobic and hydrophilic (G2REO) groups form a type of honeycomb structure (Figure 5d), the distance from the center of the honeycomb to another neighboring center is approximately 7.3 ± 0.5 nm (the pore is not a very regular structure), and pore size is 3.4 ± 1.5 nm. Figure 5c shows the magnified image of G2REO. In this image, the honeycomb structures are distributed homogeneously on the terraces of gold, indicating that ordered structures can extend over large areas. The enlarged image of Figure 5c is shown in Figure 5d. The inset is the spectrum 2D image. The six points align in a hexagonal pattern, which can be correlated with the honeycomb structure of G2REO. The formation of this honeycomb structure can be attributed to the local aggregation behavior of the hydrophobic and hydrophilic peripheries based on the like-to-like principle, if we ignore the chemisorption and $\pi-\pi$ stacking. For the above-mentioned three compounds, chemisorption and $\pi-\pi$ stacking are quite similar, leaving us to conclude that it is the peripheral substituent that contributes to the variation in surface morphology from the striped, homogeneous structure to the honeycomb structure on Au(111).

For comparison, we also examined the aggregation behavior of a 1:1 mixture of G2R and G2EO. In this case, the relative ratio between R and EO is in accordance with the dendron in a confined state (G2REO). Only random pore structures could be observed from the STM image (Figure 5e), which means the mixtures of G2R and G2EO exhibit a kind of coadsorption behavior, resulting in disordered alignment on Au(111). The considerable difference between the images of the 1:1 mixture and those of the confined dendron may indicate that the precisely tailored structure of surface-bound dendron with locally controlled hydrophobicity allows a nanophase separation in confined state, leading to the formation of the energetically favorable honeycomb structure (Figure 5d). The surface composition of the mixed monolayer at the gold covered substrate was determined by X-ray photoelectron spectroscopy (XPS). The XPS data revealed that in the mixed monolayer, the layer composition is almost the same as the solution one. We also examined the SAMs with R to EO ratios of 3:1 (1 mol G2R mixed with 1 mol G2REO) and 1:3 (1 mol G2REO mixed with 1 mol G2EO), and observed similar disordered pores. Interestingly, introducing even a small amount of a second component (for example, 20 mol G2REO mixed with 1 mol G2R), destroys the order (Figure 5f), although some orientation could also be observed from the spectrum 2D image (Figure 5f inset).

For surface-bound dendrons with hydrophilic groups, hydrogen bonds formed in aqueous solution between the oxygen atoms of the EO groups and the hydrogen atoms of water.[21] The hydrogen bonding results in a more densely packed structure, which impedes the approach of the electrochemical probe to the gold electrode. Because of the variation in the fraction of peripheral hydrophilic constituents, we found the strongest hydrogen bonding in the SAMs of G2EO, that in the SAMs of G2REO was weaker, and none was observed in the SAMs of G2R. Owing to the reasons above, ΔE_p increases, and I_p and $(1-\Theta)$ decrease from G2R/Au to G2REO/Au to G2EO/Au (Figure 6). Figure 7 summarizes the complex impedance results. The diameter increases and k^o decreases in the order of G2R/Au, G2REO/Au, and G2EO/Au, which is in accordance with the results of cyclic

a)

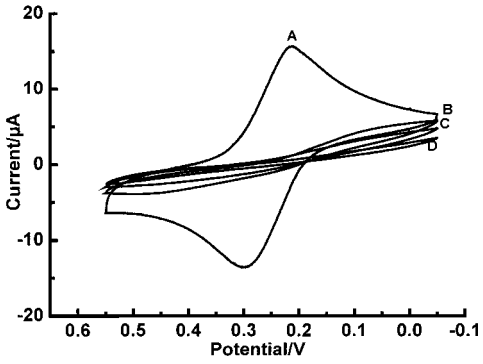

b)

	Au (A)	G2R(B)	G2REO(C)	G2EO(D)
E_{pc}/V	0.211(0.008)	0.081(0.009)	0.077(0.013)	0.048(0.009)
E_{pa}/V	0.299(0.011)	0.428(0.012)	0.434(0.015)	0.517(0.021)
I_{pc}/(μ A)	13.0(0.5)	0.96(0.07)	0.31(0.05)	0.28(0.09)
I_{pa}/(μ A)	-14.0(0.8)	-0.97(0.09)	-0.49(0.06)	-0.21(0.04)
ΔE_p/V	0.088	0.347	0.357	0.469
(1- Θ)		0.110	0.041	0.021
C_{dl}/(10^{-8}F)		30.84(0.98)	12.39(1.20)	70.96(4.68)
C_m/(10^{-8}F)		1.528	1.462	1.499
d/nm		2.7	2.9	2.8

Figure 6. a) Cyclic voltammograms of bare Au (A), G2R/Au (B), G2REO/Au (C), G2EO/Au (D) electrodes in the solution of 2 mM $K_3[Fe(CN)_6]$ + 0.1 M KCl with a scan rate of 0.10 V s^{-1}. b) Voltammetric results summarized for the electrodes.

a)

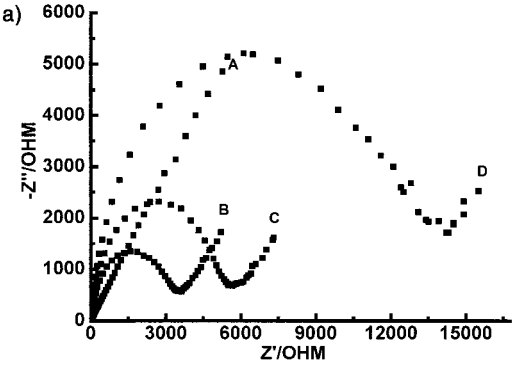

b)

	G2R(B)	G2REO(C)	G2EO(D)
R_{sq}/Ω	38.8(9.5)	37.5(8.2)	44.9(1.8)
R_{ct}/Ω	2885(67)	4793(88)	10763(325)
k°/(10^{-6}m s^{-1})	5.9	3.5	1.6

Figure 7. a) Complex impedance plots of bare Au (A), G2R/Au (B), G2REO/Au (C), and G2EO/Au (D) electrodes in 5 mM $K_4[Fe(CN)_6]$ + 5 mM $K_3[Fe(CN)_6]$ + 0.5 M KCl aqueous solution. b) AC impedance results for the electrodes.

voltammetric measurements. In addition, based on the capacitance, the monolayer thickness can be calculated as shown in Figure 6b .

We compared adsorbates dimensions of D3,3 and G2R with the corresponding data obtained by STM and electrochemical analysis to understand the molecular orientation on surface. Based on the molecular mechanics method (MM2), the dimension of the molecule D3,3 is calculated to be 1.69 nm for its widest part and 1.2 nm for its highest part; whereas G2R is 1.95 nm and 1.6 nm, respectively. These data confirm that the introduction of alkyl chains expand the molecular dimensions. The increase of the molecular dimensions from D3,3 to G2R is consistent with the increase of stripe widths of the SAMs on the gold surface. However, the molecular dimensions of the dendrons are smaller than the stripe width measured by STM. This is because in the computational simulation the molecule has the tendency to backfold to adopt a less extended conformation. But at the gold surface, these molecules would prefer an extended conformation due to the collective interaction of chemisorption and intermolecular interaction. This postulation sounds reasonable when we compare their thickness. The monolayer thickness calculated for D3,3 (1.6 nm) is a little bit larger than its simulated one, indicative of an orientated monolayer adsorption on gold substrate. Comparing the thickness calculated for D3,3 (1.6 nm) and G2R (2.7 nm), it is reasonable to see that the SAMs of G2R become thicker than D3,3 due to the introduction of alkyl chains at the periphery. However, the monolayer thickness calculated for G2R is larger than the simulated one (1.6 nm). This comparison infers that G2R is orientated after the chemisorption at the gold surface, which agrees well with our assumption that the introduction of alkyl chains can enhance the interaction between symmetrical backbones.

Conclusion

Novel surface-bound dendrons that maintain the active site of the alkanethiol, but with the thiol group connected to different groups through a dendritic linkage, have been synthesized and their aggregation behavior on gold substrates have been studied by STM and electrochemical measurements. The precisely tailored structures of surface-bound dendrons with different main structures and peripheral substituents have allowed the formation of some special surface structures on gold. Among the factors that influence the aggregation behavior, chemisorption is quite similar for these compounds. Therefore, it is the intermolecular interaction that greatly affects the configuration of these molecules on gold as shown by the results of both STM and electrochemical measurements: for example, the different results obtained from SAMs composed of symmetrical and asymmetric structures, the different aggregation behavior influenced by peripheral substituents, and the coadsorption process. Such controllable results may not only enrich the field of SAMs but also promote the further exploration in non-alkane based SAM systems (especially surface-bound dendrons) and even some new applications.

Experimental Section

General: THF was distilled from sodium before use. Other chemicals were analytical-grade reagents and were used as received. ^{1}H NMR spectra were recorded in $CDCl_3$ on a Bruker Advance 500(500 MHz) spectrometer using a TMS proton signal as the internal standard. IR spectra were recorded on an ISF-66V spectrometer on a CaF slide. Elemental analyses were obtained on Flash EA 1112, Thermo Quest. X-ray photoelectron spectroscopy was performed on a VG-Escalab Mark spectrometer with an $Al_{K\alpha}$ monochromated X-ray source, and a modified gold slide as the substrate. STM images were obtained from a commercial instrument (Digital Instruments, Multi-

mode nanoscope IIIa). Tunneling parameters of 750 mV (bias voltage) and 500 pA (current set point) were used for recording images if not otherwise indicated. Electrochemistry was carried out in a conventional three-electrode glass electrochemical cell. The auxiliary electrode was platinum and the reference electrode was an Ag/AgCl (saturated KCl) electrode. Cyclic voltammetry measurements were performed on a CHI 832 Electrochemical Instrument (CHI Inc., USA) in 2 mM $K_3[Fe(CN)_6] + 0.1$ M KCl (scan rate 0.10 $V s^{-1}$). AC impedance measurements were performed on a Solartron 1470 Battery Test Unit and a Solartron 1255 B Frequency Response Analyzer (Solartron Inc., England) in 5 mM $K_4[Fe(CN)_6] + 5$ mM $K_3[Fe(CN)_6] + 0.5$ M KCl aqueous solution. A sinusoidal potential modulation with an amplitude of ± 5 mV was superimposed on the formal potential (0.22 V versus Ag/AgCl (saturated KCl)) of the redox couple of $[Fe(CN)_6]^{4-}/[Fe(CN)_6]^{3-}$. The impedance data were fitted with an equivalent circuit using the *Z* plot/*Z* view software (Scribner Associates Inc., England). The equivalent circuit provided an electrical analogue of the chemical/physical processes probed by AC EIS.

Preparation of self-assembled monolayers on gold used for STM characterization: Quartz substrates supplied were thoroughly cleaned prior to use; they were precoated with 6 nm chromium followed by 130 nm gold. Both were evaporated at a pressure of 5×10^{-6} mbar in a heated tungsten boat. The resulting gold slides were flame-annealed at about 1000 K for about one minute.[22] Such treatment often produced large areas of Au(111) terraces, often extending over thousands of angstroms. The gold slide was subsequently dipped into the THF solution of the surface-bound dendrons (1×10^{-3} M), removed after immersion for 24 h, and dried before characterization.

Preparation and characterization of surface-bound dendrons: The synthesis and characterization of G2R, G2REO, G2EO, and D3,3 were described elsewhere.[16, 17] Fréchet-type dendritic bromides bearing benzene groups at their periphery were selected as the starting materials. In a similar way,[18–20] we synthesized the asymmetric dendritic bromides of D1,3 and D3,7. Asymmetric surface-bound dendrons were prepared by thiourea substitution of the corresponding dendritic bromides as described previously.[16, 17]

D1,3: IR (CaF): $\tilde{\nu} = 3032$ (Ar-H), 2927, 2871 (CH_2), 1595 (Ar C=C), 1155 (Ar–O), 1053 cm^{-1} (C-O-C); ^{1}H NMR ($CDCl_3$, 500 MHz):$\delta = 7.42 - 7.32$ (m, 15H; C_6H_5), 6.67 – 6.48 (m, 6H; C_6H_3), 5.04 – 4.96 (m, 8H; OCH_2Ar), 3.67 – 3.66 (d, 2H; SCH_2Ar), 1.76 ppm (t, 1H; SH); elemental analysis (%) for $C_{35}H_{33}O_4S$ (549.7): calcd: C 76.47, H 6.05, S 5.83; found: C 76.44, H 6.16, S 6.13.

D3,7: IR: $\tilde{\nu} = 3032$ (Ar–H), 2917, 2869 (CH_2), 1595 (Ar C=C), 1153 (Ar–O), 1051 cm^{-1} (C-O-C); ^{1}H NMR ($DCCl_3$): $\delta = 7.41 - 7.29$ (m, 30H; C_6H_5), 6.68 – 6.48 (m, 15H; C_6H_3), 5.02 – 4.94 (m, 20H; O CH_2 Ar), 3.65 – 3.64 (d, 2H; SCH_2Ar), 1.75 ppm (t, 1H; SH); elemental analysis (%) for $C_{77}H_{68}O_{10}S$ (1185.4): calcd: C 78.02, H 5.78, S 2.70; found: C 77.97, H 5.95, S 3.00.

Electrochemical measurements: A bare gold electrode (Au wire sealed in polytrifluoroethylene) was pretreated as follows: the gold electrode was mechanically polished with 1 μm, 0.3 μm, and 0.05 μm α-Al_2O_3 and washed ultrasonically with doubly distilled water. Next, it was electrochemically cleaned in 1M H_2SO_4 by potential scanning between -0.2 and 1.55 V until a reproducible cyclic voltammogram was obtained, and then completely rinsed with doubly distilled water and ethanol. Finally, it was dried with high-purity nitrogen before monolayer adsorption. The monolayers were formed by placing the bare gold electrode in a 1 mM solution of the dendron in THF for 24 h at room temperature. Thereafter, the gold electrode modified with dendron was rinsed with ethanol and dried before further characterization. The monolayer thickness was calculated based on electrochemical data (capacitance). It is reasonable to assume as a simple approximation that C_{dl} is a parallel combination of the double-layer capacitance C_{Au} in the pinholes and the monolayer capacitance C_m, thus providing Equation (1) for the evaluation of C_m.[23], and the monolayer

$$C_m = (C_{dl} - C_{Au} \times (1 - \Theta))/\Theta \quad (1)$$

thickness *d* can be then calculated by using the monolayer dielectric constant ε_m,[24] where $C_{Au} = 2.680 \times 10^{-6}$ F. $C_m = A\varepsilon_m \times \varepsilon_o/d$, where $A = 3.14 \times 10^{-6}$ m^2, the geometric area of gold electrode; $\varepsilon_m = 1.5$, the monolayer dielectric constant; $\varepsilon_o = 8.854 \times 10^{-12}$ $F m^{-1}$, the vacuum dielectric constant.

Acknowledgement

We thank the Major State Basic Research Development Program (Grant. No. G2000078102), Key Project of the Ministry of Education and National Natural Science Foundation of China 20074014, 29992590 – 5, 59928303 for financial support. We also thank Dr. Barbara Whitesides for helping in editing our English and Dr. Lifeng Chi for helping with the STM characterization. The very helpful comments from the referee are greatly acknowledged.

[1] For reviews see, for example: a) O. S. M. Grayson, J. M. J. Fréchet, *Chem. Rev.* **2001**, *101*, 3819 – 3867; b) H. J. van Manen, F. C. J. M. van Veggel, D. N. Reinhoudt, *Top. Curr. Chem.* **2001**, *217*, 121 – 162; c) G. R. Newkome, E. He, C. N. Moorefield, *Chem. Rev.* **1999**, *99*, 1689 – 1746; d) A. W .Bosman, H. M. Janssen, E. W. Meijer, *Chem. Rev.* **1999**, *99*, 1665 – 1688; e) M. Fischer, F. Vögtle *Angew. Chem.* **1999**, *111*, 934 – 955; *Angew. Chem. Int. Ed.* **1999**, *38*, 884 – 905; f) O. A. Matthews, A. N. Shipway, J. F. Stoddart, *Prog. Polym. Sci.* **1998**, *23*, 1 – 56; g) H. F. Chow, T. K. K. Mong, M. F. Nongrum, C. W. Wan, *Tetrahedron* **1998**, *54*, 8543 – 8660; h) F. Zeng, S. C. Zimmerman, *Chem. Rev.* **1997**, *97*, 1681 – 1712; i) G. R. Newkome, C. N. Moorefield, F. Vögtle, *Dendritic Macromolecules: Concepts, Syntheses, Perspectives*, VCH, Weinheim, **1996**.

[2] J. W. J. Knapen, A. W. van der Made, J. C. de Wilde, P. W. N. M. van Leewen, P. Wijkens, D. M. Grove, G. van Koten, *Nature* **1994**, *372*, 659 – 663.

[3] D. Astruc, F. Chardac, *Chem. Rev.* **2001**, *101*, 2991 – 3023.

[4] R. Roy, D. Zanini, S. J. Meunier, A. Romanowska, *J. Chem. Soc. Chem. Commun.* **1993**, 1869 – 1872.

[5] L. A. J. Chrisstoffels, A. Adronov, J. M. J. Fréchet, *Angew. Chem.* **2000**, *112*, 2247 – 2251; *Angew. Chem. Int. Ed.* **2000**, *39*, 2163 – 2167.

[6] D. C. Tully, K. Wilder, J. M. J. Fréchet, A. R. Trimble, C. F. Quate, *Adv. Mater.* **1999**, *11*, 314 – 318.

[7] D. C. Tully, A. R. Trimble, J. M. J. Fréchet, K. Wilder, C. F. Quate, *Chem. Mater.* **1999**, *11*, 2892 – 2898.

[8] T. Nakamura, H. Kondoh, M. Matsumoto, H. Nozoye, *Langmuir* **1996**, *12*, 5977 – 5979.

[9] A. Dhirani, R. W. Zehner, R. P. Hsung, P. Guyot-sionnest, L. R. Sita, *J. Am. Chem. Soc.* **1996**, *118*, 3319 – 3320.

[10] G. E. Poirier, *Chem. Rev.* **1997**, *97*, 1117 – 1127.

[11] S. Flink, F. C. J. M. van Veggel, D. N. Reinhoudt, *Adv. Mater.* **2000**, *12*, 1315 – 1328.

[12] R. M. Crooks, A. J. Ricco, *Acc. Chem. Res.* **1998**, *31*, 219 – 227.

[13] M. Á. Herranz, B. Colonna, L. Echegoyen, *Proc. Natl. Acad. Sci. USA* **2002**, *99*, 5040 – 5047.

[14] C. B. Gorman, R. L. Miller, K. Y. Chen, A. R. Bishop, R. T. Haasch, R. G. Nuzzo, *Langmuir* **1998**, *14*, 3312 – 3319.

[15] Z. S. Bo, L. Zhang, B. Zhao, X. Zhang, J. C. Sheng, S. Höppener, L. F. Chi, H. Fuchs, *Chem. Lett.* **1998**, 1197 – 1198.

[16] L. Zhang, F. W. Huo, Z. Q. Wang, L. X. Wu, X. Zhang, S. Höppener, L. F. Chi, H. Fuchs, J. W. Zhao, L. Niu, S. J. Dong, *Langmuir* **2000**, *16*, 3813 – 3817.

[17] L. Zhang, B. Zou, B. Dong, F. W. Huo, X. Zhang, L. F. Chi, L. Jiang, *Chem. Commun.* **2001**, 1906 – 1907.

[18] C. L. Hawker, J. M. J. Fréchet, *Macromolecules* **1990**, *23*, 4726 – 4729.

[19] K. L. Wooley, C. J. Hawker, J. M. J. Fréchet, *J. Chem. Soc. Perkin Trans. 1* **1991**, 1059 – 1076.

[20] C. J. Hawker, J. M. J. Fréchet, *J. Am. Chem. Soc.* **1992**, *114*, 8405 – 8413.

[21] C. Miller, P. Cuendet, M. Grätzel, *J. Phys. Chem.* **1991**, *95*, 877 – 886.

[22] W. Haiss, D. Lackey, J. K. Sass, K. H. Besocke, *J. Chem. Phys.* **1991**, *95*, 2193 – 2196.

[23] E. Sabatani, I. Rubinstein, R. Maoz, J. Sagiv, *J. Electroanal. Chem.* **1987**, *219*, 365 – 371.

[24] D. M. Pomerantz, A. Segmuller, L. Netzer, J. Sagiv, *Thin Solid Films* **1985**, *132*, 153 – 162.

Received: October 8, 2002 [F4483]